

Article

Investigation on Spectral Characteristics of Gliding Arc Plasma Assisted Ammonia Lean Combustion

Ximing Zhu ¹, Yang Zhao ^{1,*}, Ming Zhai ¹, Pengyi Lv ¹, Weixing Zhou ¹ and Bangdou Huang ^{2,*} ¹ School of Energy Science and Engineering, Harbin Institute of Technology, Harbin 150001, China² Beijing International S&T Cooperation Base for Plasma Science and Energy Conversion, Institute of Electrical Engineering, Chinese Academy of Sciences, Beijing 100190, China

* Correspondence: zhaoyang97@hit.edu.cn (Y.Z.); huangbangdou@mail.iee.ac.cn (B.H.)

Abstract: Ammonia as a non-carbon fuel is expected to play an important role in the future, but it is difficult to be effectively utilized at this stage due to its flame retardancy and other characteristics. Therefore, we propose to use gliding arc plasma combined with a swirl burner to enhance the combustion performance of ammonia. The electrical characteristics, electron density, gas rotational temperature and the distribution of key active species in the burner were studied via optical emission spectroscopy (OES). With the increase of equivalence ratio (EQR), the width of the H α line decreases significantly, indicating that the electron density shows a downward trend, even as the gas rotational temperature shows an upward trend. When the equivalence ratio was 0.5, the gas rotational temperature increases by about 320 K compared with the pure air condition. During pure air discharge, there will still be obvious NO emission due to the plasma reaction, but with the addition of NH₃, the NO content in the emission is significantly reduced. The light intensity of O atoms in the burner gradually decreases with the increase of the equivalence ratio, the light intensity of H atoms increases first and then decreases, and the light intensity of NH shows an upward trend. The reason may be that the plasma discharge effectively strengthens NH₃(E)→NH₂+H, NH₂+H→NH+H₂ and other reactions promote the initial reaction step of NH₃ which thus effectively strengthens the NH₃ combustion.

**Citation:** Zhu, X.; Zhao, Y.; Zhai, M.;

Lv, P.; Zhou, W.; Huang, B.

Investigation on Spectral

Characteristics of Gliding Arc Plasma

Assisted Ammonia Lean Combustion.

Processes **2022**, *10*, 1750. [https://](https://doi.org/10.3390/pr10091750)doi.org/10.3390/pr10091750

Academic Editor: Albert Ratner

Received: 10 August 2022

Accepted: 30 August 2022

Published: 2 September 2022

Publisher's Note: MDPI stays neutral with regard to jurisdictional claims in published maps and institutional affiliations.



Copyright: © 2022 by the authors. Licensee MDPI, Basel, Switzerland. This article is an open access article distributed under the terms and conditions of the Creative Commons Attribution (CC BY) license (<https://creativecommons.org/licenses/by/4.0/>).

Keywords: gliding arc; swirl burner; ammonia combustion; spectrum

1. Introduction

With the rapid development of the world economy, the problem of CO₂ emissions caused by the use of large amounts of fossil fuels has become increasingly prominent [1]. Excessive CO₂ emissions have brought a series of environmental problems such as the greenhouse effect. In order to solve these problems effectively, many scientists have proposed a variety of technologies to curb CO₂ emissions. In recent years, ammonia has attracted the attention of many scholars as a zero-carbon fuel [2–4]. Ammonia has the characteristics of easy production, storage and transportation. It can store and transport energy that is difficult to use effectively such as wind and solar at a low cost, and release energy through burning, thus it is a very promising zero-carbon fuel [5,6]. However, ammonia as a fuel has the disadvantages of long ignition delay time, low flame propagation speed, small flammable range, and easy generation of a large amount of nitrogen oxides during combustion, which limits the large-scale utilization of ammonia as a fuel [7–9]. In order to effectively solve these problems, scholars have proposed a variety of technologies. Among these, the use of low-temperature plasma to assist ammonia combustion is one of the more feasible solutions [10,11].

In the past few decades, plasma has shown great potential in enhancing ignition and flame stability and has received great attention from researchers in the field of combustion [12]. In addition to simple heating of air-fuel, the use of non-equilibrium plasma can generate many chemically active species, such as excited state molecules and active free radicals, these active species will promote a branch reaction, thereby accelerating the

chemical reaction process [13]. At the same time, the discharge will decompose some large fuel molecules into small fuel fragments, and the electric field between the electrodes drives the fluid to flow [14]; thus, the ion wind formed between the two electrodes also accelerates the mixing of fuel and oxidant [15], which all contribute to the progress of chemical reactions and enhance the ignition and burning processes. Wu et al. [16] studied an ethylene coaxial jet laminar flame. In the study, O_3 was generated by plasma discharge, and the spatial distribution of CH_2O in the flame was investigated by PLIF. The results show that even a small amount of O_3 (2000 ppm) generated by plasma discharge will have a great impact on the flame propagation speed and flame lift-off height of the ethylene flame, and the addition of O_3 will greatly promote the conversion of C_2H_4 to CH_2O . Shanbhogue et al. [17] used nanosecond pulsed discharge plasma to study syngas turbulent flames under pressurized conditions. Their results show that under pressurized conditions, especially in a lean burn flame, the introduction of nanosecond pulse discharge plasma can effectively improve the blow-out limit of the syngas flame and improve the stability of the flame. At the same time, the addition of pulsed discharge plasma at 25 kHz can also reduce the pressure fluctuation amplitude under lean premixed conditions by more than 40%, which can significantly improve the combustion characteristics under lean combustion conditions. Zhao et al. [18] conducted an experimental study on the ignition characteristics of aviation kerosene. Their results show that a large number of O atoms and CH radicals will be generated in a short time when the plasma torch is used for ignition. At the same time, compared with the traditional spark ignition, the minimum ignition delay time can be shortened by 88.74%, and with the increase of plasma current, the ignition delay time will be further shortened. Chen and Deng et al. [19,20] studied the effect of plasma discharge on flame stability through experiments, and their results show that ionization played a role in heating the flame, thereby effectively reducing its instability.

Therefore, the introduction of low-temperature plasma can effectively generate a large amount of active species and improve the stability of the flame and combustion parameters, and it is expected to play its unique advantages in solving the combustion problem of ammonia.

Li and Sun et al. [10,11] used a gliding arc discharge and nanosecond pulse plasma to conduct experimental research on the combustion characteristics of ammonia and found that the introduction of plasma can effectively broaden the lean burn limit and increase blowout limit for ammonia premixed flames. At the same time, it was also found that plasma discharge can reduce NO_x emissions in ammonia combustion, which is different from common hydrocarbon fuels. At present, the mechanism of plasma discharge reducing NO_x emissions in ammonia combustion is still unclear. However, according to the detection results of NH_2 -PLIF, it is inferred that more radicals such as NH_2 are generated in the plasma discharge, which promotes the reduction reaction of nitrogen oxides such as $NH_2 + NO = N_2 + H_2O$ and inhibits the formation of nitrogen oxides in the flame.

In summary, the use of low-temperature plasma-assisted combustion technology has made great progress in the past few decades, and has produced important applications in energy, aerospace and other fields, and the mechanism of hydrocarbon combustion has been relatively clear. However, existing research on NH_3 combustion is still in the qualitative research stage of the overall effect of a simple experimental bench, and the discharge and combustion mechanisms of low-temperature plasma-assisted ammonia combustion are still unclear.

In this paper, key parameters, such as the generated excited H atoms, O atoms, and the gas rotational temperature of the NH_3 /AIR mixture gas under different equivalence ratios, were experimentally studied by using optical emission spectroscopy (OES) combined with the filter imaging method. The influence of gliding arc plasma on ammonia combustion was studied, and its action mechanism was preliminarily discussed.

2. Experimental Setup

2.1. Gliding Arc Plasma Equipment and Swirl Burner

In this experiment study, the structure of the gliding arc discharge equipment and swirling burner is shown in Figure 1. The main structure is composed of a spindle-shaped inner electrode at the center, a cylindrical outer wall and four nozzles at the bottom. The NH_3 and air were firstly mixed uniformly in the premixing tank and then uniformly entered into the bottom of the burner through the four-way intake pipes. The four nozzles are staggered at the bottom of the burner, and the mixed gas flow interacts with each other and is restricted by the cylindrical outer wall to produce a strong swirl effect. The rotating mixed gas flow moves upwards, producing obvious discharges at the narrow places passing through the center electrode and the outer wall, and the arc rotates upwards along with the mixed gas flow, resulting in a gliding arc plasma effect.

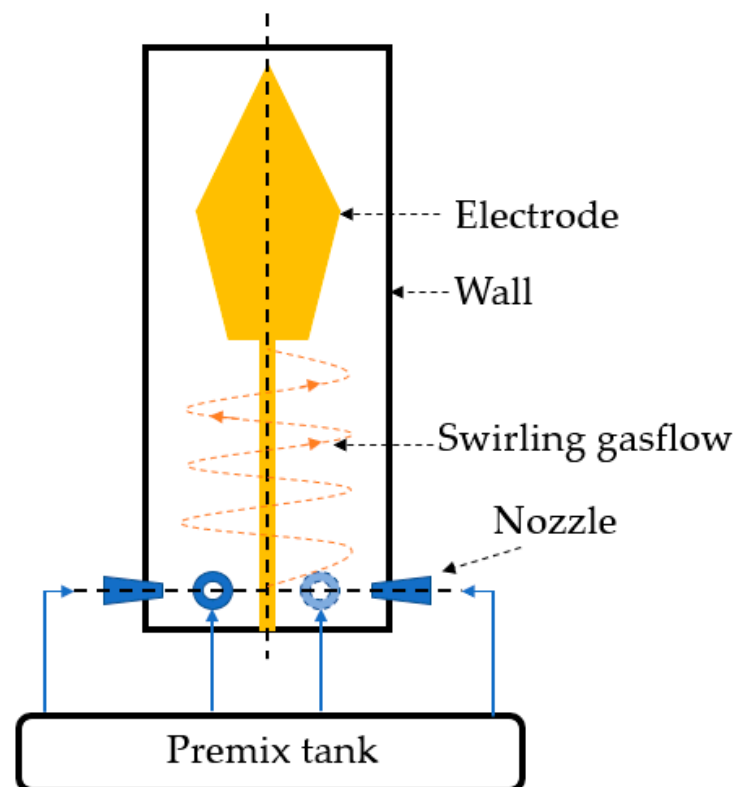


Figure 1. Structural diagram of the gliding arc discharge equipment and swirling burner.

2.2. Experimental System

The overall system of the experiment is shown in Figure 2. The mixed gas enters the burner from the lower nozzle after being mixed in the premix tank. The power supply used in the experiment is AC power, the high-voltage output is connected to the center electrode, and the outer wall is grounded. The specific parameters of the power supply are as follows: the output voltage range is 0–30 kV, the AC frequency is continuously adjustable between 5–20 kHz, and the stable output power of the power supply is 0–500 W.

2.2.1. Electrical Measurements

The 1000:1 capacitor voltage divider is used to step down the output signal of the high-voltage power supply, and then the oscilloscope (YOKOGAWA DL350, Tokyo, Japan) is used to collect its current and voltage signals, and the collected current and voltage signals are used to obtain information such as instantaneous power and average power. The calculation formulas of instantaneous power and average power are as follows:

$$P(t) = U(t)I(t) \quad (1)$$

$$P_{avg} = \frac{\int_0^{t_1} U(t)I(t)dt}{t_1} \quad (2)$$

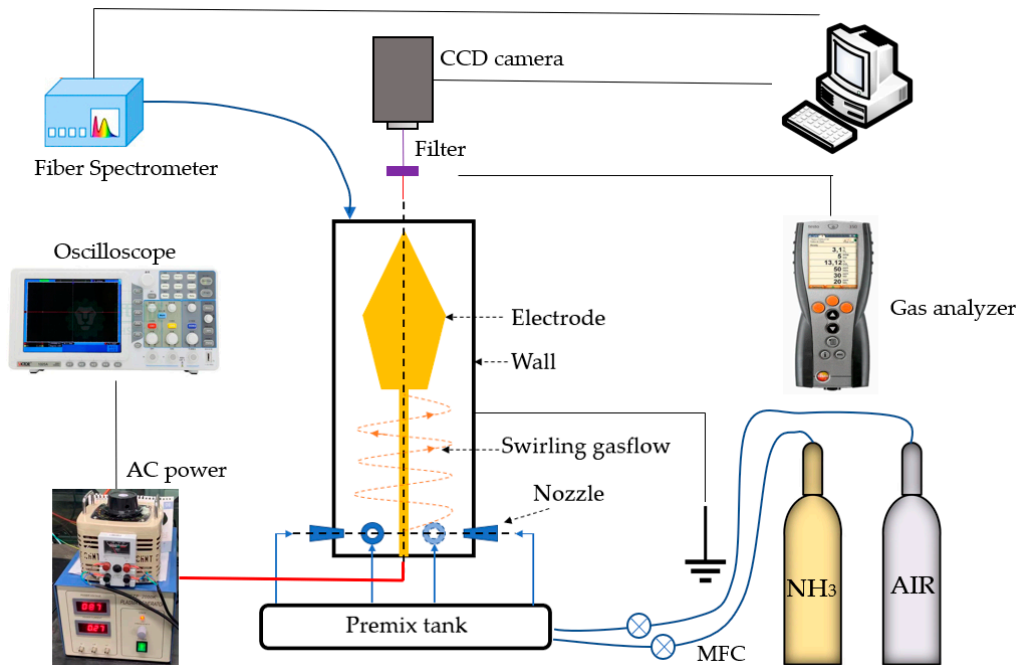


Figure 2. Experimental system.

2.2.2. Emission Spectrometry

In order to explore the influences of equivalence ratio on the change of electron density and excited state substances during the discharge and combustion process, a fiber optic spectrometer was used to collect the axial spectrum inside the burner at the exit position of the burner. The collection position is shown in Figure 3. The spectrometer used in the experiment was an Avantes 2048FT 8-channel spectrometer (Apeldoorn, Netherlands), the effective wavelength range of the spectrometer was 200–1100 nm, and the spectral resolution was 0.05 nm. Before the experiment, the spectrometer was utilized with an Avantes standard lamp, and the collected data were obtained by the average of four data collections, each obtained under the same working conditions.

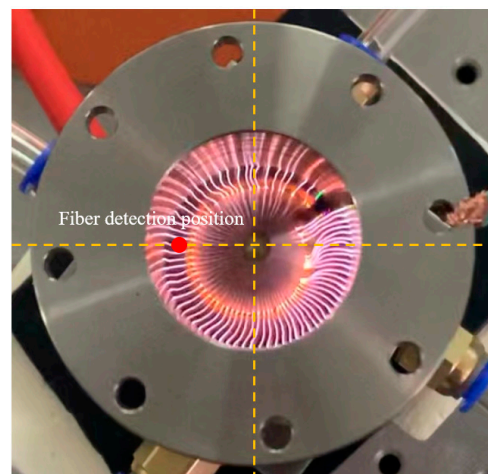


Figure 3. Spectrum collection location.

2.2.3. Imaging System

In order to explore the spatial distribution of plasma and flame and the spatial distribution of key excited substances in the gliding arc swirl burner, a CCD camera and filters of different wavelengths were set above the burner to collect images in the axial direction inside the burner. The images captured by the camera were obtained by averaging five photos. The central wavelengths of the filters used for collection were 660 nm and 780 nm and the bandwidth are 5 nm, corresponding to the emission wavelengths of H_{α} (656 nm) and $O777$, respectively.

2.2.4. Gas Analyzer

The nitrogen oxides in the flue gas were sampled with a gas analyzer (testo 340), and the collection position was at the center of the burner outlet. The NO_x emissions were normalized to 15% O_2 in the exhaust gas [21,22] by the following formula:

$$X_{15,i} = X_i \frac{20.9 - 15}{20.9 - X_{O_2}} \quad (3)$$

where X_i is the measured mole fraction of species i ; $X_{15,i}$ is the normalized species mole fraction at 15%, and X_{O_2} is the measured O_2 mole fraction in the exhaust gas expressed as a percentage. NO is the most abundant substance in nitrogen oxides produced in the process of discharge and combustion, and it has a very strong effect on environmental pollution [23,24]. Therefore, in this paper, a NO sensor is installed in the flue gas analyzer to detect the NO content in the flue gas.

3. Results and Discussion

3.1. Electrical Characteristics

When high-voltage AC power is used to act on the gliding arc device to generate plasma, the change of the working medium composition will affect the parameters such as current, voltage and power during the discharge process. Therefore, this paper uses the oscilloscope (YOKOGAWA DL350, Tokyo, Japan) to record the current and voltage signals. The instantaneous power and average power were also calculated.

The current and voltage during the discharge process are shown in Figure 4a. Under different conditions, the voltage peak is about 4 kV. When the gas in the gliding arc device gets broken down and generates plasma, the voltage waveform changes greatly. When the AC voltage reaches the peak value, it drops rapidly as breakdown happens, and it keeps fluctuating around a lower value for a long time and then continues to change. A strong current pulse is generated only when breakdown happens and the current is maintained at tens of milliamps for a long time.

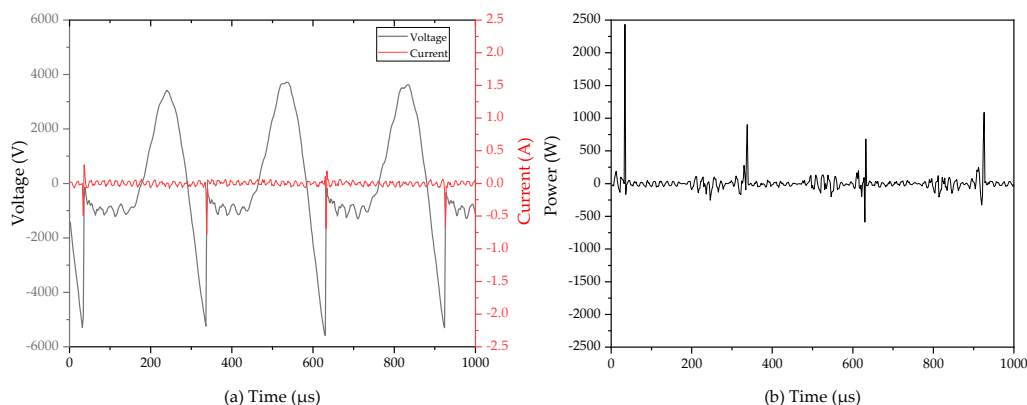


Figure 4. (a) Discharge waveforms and (b) instantaneous power of gliding arc plasma.

Figure 4b shows the instantaneous power output by the plasma power supply. It can be seen from the figure that only a large instantaneous power appears for a very short time corresponding to the peak voltage and current.

Table 1 shows the average output power when the equivalent ratio is 0–0.5. In this experiment, we control the air flow constant (12 slm) and control the equivalence ratio change by adjusting the ammonia flow. It can be seen from Table 2 that the average output power is generally at a low level, but the values under different working conditions still show some difference. Among these, when the equivalence ratio is 0.5, the output power is the highest, which is 5.13 W. Under other working conditions, the electric power is about 4 W. The difference in electric power leads to the difference in the heating effect of Joule heat on the mixed gas flow during the discharge process. Stronger electric power will produce a significant gas heating effect and increase the temperature of the mixed gas. Effective ignition can be achieved when the equivalence ratio is 0.5 with a low electrical power, which broadens the lean combustion limit of the ammonia swirl flame and has a better economy.

Table 1. Main symbols in this article and their meanings.

Symbol	Meaning
EQR	Equivalence ratio
OES	Optical emission spectroscopy
H_{α}	The spectral line of H with a wavelength of 656.28 nm
$P(t)$	Instantaneous power
P_{avg}	Average power
n_0	Refractive index of air
Y_{pq}^C	Rovibrational transition parameters of $N_2 C^3\Pi_u$
Y_{pq}^B	Rovibrational transition parameters of $N_2 B^3\Pi_g$
D	Proportionality constant of a transition
H, c, K	Planck's constant, speed of light, Boltzmann constant
B	Rotational dynamic constant
H	Hall-London factor
$\Delta\lambda$	Difference from the center wavelength of the rotational peak
W	The half-height width of the rotational peak (width broadens to $\pm Wa^{0.5}$).
$q_{v',v''}$	Frank-Condon factor
$\omega_e, \omega_e x_e$	Vibration constant
T_r, T_v	Rotational temperature, vibration temperature
E_J	Rotational energy at higher rotational energy levels
$B_{v'}$	Rotational dynamic constant

Table 2. Average output power of gliding arc plasma.

EQR	0	0.1	0.2	0.3	0.4	0.5
Power (W)	4.31	3.71	4.20	3.65	3.32	5.13

3.2. Spectral Characteristics of Gliding Arc Plasma

Plasma-assisted gas combustion is mainly achieved by enhancing the reaction kinetics and thermodynamics and by enhancing the transport characteristics of fuel and oxidant mixing. In this study, ammonia and air were premixed through a premix tank before entering the swirl burner. This research mainly focuses on the active species and thermal effects generated by plasma discharge.

Figure 5 shows the spectral signal obtained using the spectrometer to detect the main discharge (burning) position of the gliding arc swirl burner. It can be seen from the spectral data that a large number of N atoms, O atoms and excited N_2 are generated in the air during the discharge process. With the addition of NH_3 , H lines and an NH band appeared, this shows that a considerable number of O atoms, H atoms and other active particles are generated during the discharge process, which is crucial to the combustion of NH_3 , and

NH₃ will also effectively dissociate to generate NH and other radicals during the discharge process [25]. It can be seen that with the increase of equivalent ratio, the integrated light intensity value of the N₂ bands only show a small fluctuation, while the light intensity values of O and N atoms show an obvious downward trend, the light intensity of H atoms generally increase first and then decrease, and the light intensity of NH shows an overall upward trend. The reason may be that with the increase of NH₃, the reaction R1 has been greatly enhanced, and a large amount of ground state NH₃ generates electronically excited NH₃ through electron collision reaction. The electronically excited NH₃ is extremely unstable and will rapidly decompose to generate NH₂ and H. Therefore, when the mixed gas contains a small amount of NH₃, the number of H atoms increases significantly; when the NH₃ is further increased, the reaction speed of R3 has been greatly improved. At the same time, with the progress of R4, the H generated by the decomposition of NH₃(E) is rapidly consumed and reacts with NH₂ to form NH, so the light intensity of H observed in the experiment begins to show a downward trend while the light intensity of NH gradually increases.

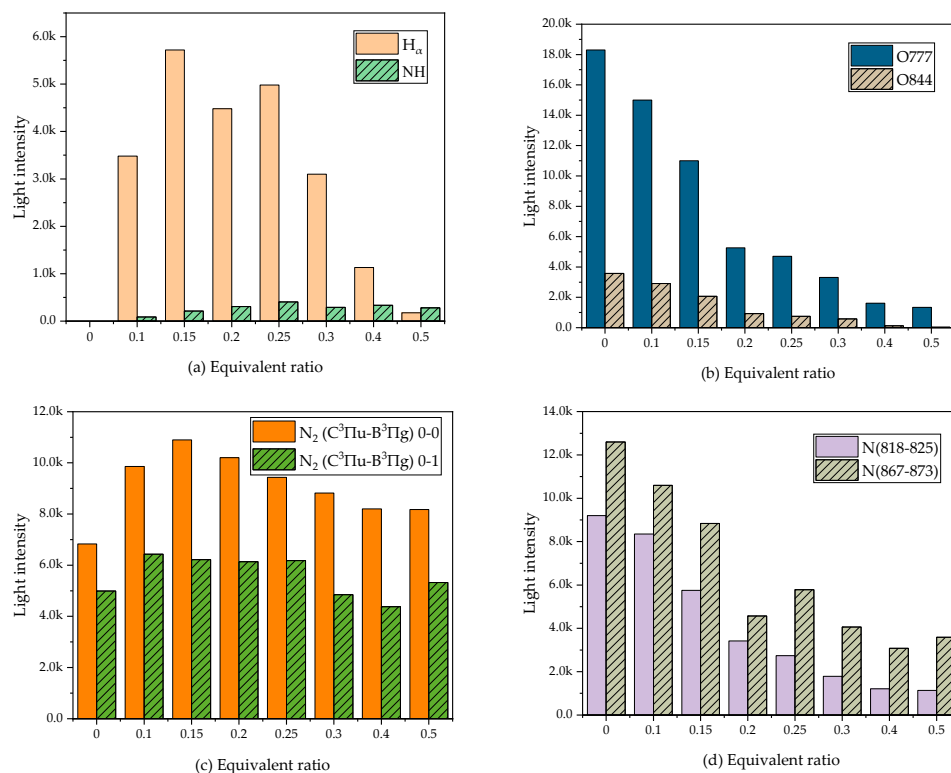
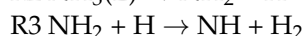
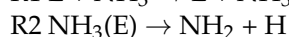
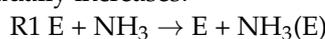


Figure 5. Integrated light intensity of different spectral lines/bands, (a) NH and H, (b) O atoms, (c) N₂, (d) N atoms.

In the plasma discharge reaction, electrons collide with heavy particles to generate a large number of free radicals and excited species, thus different types and proportions of excited species will be generated due to the different distribution of electron energy during the discharge. The general variation law of electron energy during plasma discharge can be obtained by the light intensity of the generated excited species and the excitation energy of the corresponding excited species [26,27]. In this study, there are relatively strong O777 and O844 spectral lines, therefore, the corresponding mass number density ratio of these two spectral lines is used to qualitatively characterize the variation trend of electron energy with equivalence ratio. With the increase of NH₃ in the mixed gas, the ratio shows an upward trend as a whole, but the growth trend is relatively gentle when the equivalence ratio is

0–0.3, and it begins to rise sharply when the equivalence ratio is greater than 0.3, indicating that the content of O777 begins to be significantly more than that of O844. This illustrates that the electron energy gradually decreases with the increase of equivalence ratio. The reason may be that with the increase of NH₃, the gas flow rate gradually increases, the electron collision reaction frequency increases, and the electron mean free path decreases gradually, thus the electron energy also decreases gradually.

In this study, the least squares method was used to fit the Lorentz profile of the H_α spectral line to obtain the broadening information of the H_α spectral line, which can be used to characterize parameters such as electron density under the corresponding working conditions [28].

The Lorentz profile is as follows:

$$L(\lambda) = \frac{I_{MAX}}{1 + 4 \times ([\lambda - (\lambda_0 - \lambda_d)] / \Delta\lambda_L)^2} \quad (4)$$

Under the experimental conditions, the light intensity of the H spectral line decreases significantly when the equivalence ratio is too high, so the H_α spectral line when the equivalence ratio is 0.1–0.3 is selected for fitting. The half-peak width of H_α lines are shown in Table 3. It can be seen that with the increase of NH₃, the H atom spectral line distribution gradually narrows, and the corresponding H_α spectral line broadening generally decreases, indicating that with the increase of NH₃ content, the electron density gradually decreases [29,30], thus leading to the gradual decrease in the current shown in Figure 4.

Table 3. Half-peak width of H_α lines.

EQR	0.1	0.15	0.2	0.25	0.3
Width (nm)	0.88	0.82	0.52	0.47	0.35

The rotational temperature can be obtained by fitting the spectral band of N₂. The symbols and corresponding meanings in the fitting process are shown in Table 1.

The wavelength corresponding to the transition Cv'J' → Bv''J'' of the N₂ can be expressed as

$$\lambda_{B_{v''}J''}^{C_{v'}J'} = \left\{ n_0 \sum_{p=0}^5 \sum_{q=0}^2 Y_{pq}^C \left(v' + \frac{1}{2} \right)^P [J'(J'+1)]^q - Y_{pq}^B \left(v'' + \frac{1}{2} \right)^P [J''(J''+1)]^q \right\}^{-1} \quad (5)$$

Calculate the theoretical intensity at each wavelength as follows

$$I_{B_{v''}J''}^{C_{v'}J'} = DH_J \exp[-hcB_{v'}J'(J'+1)/KT_r] \quad (6)$$

The intensity distribution of the bands is affected by the broadening of each rotational peak. To simulate line broadening, it is necessary to multiply the intensity of each spectral line by broadening, and then superimposing the vibrational and rotational peaks to form a band. In order to simplify the calculation, the finite broadening function proposed by Phillips is used to describe the broadening of the rotational peak [31]:

$$g(\Delta\lambda) = \frac{a - (2\Delta\lambda/W)^2}{a + (a-2)(2\Delta\lambda/W)^2} \quad (7)$$

In the calculation, J' = 0, . . . , 40, considering the three branches of P, Q and R corresponding to each J', the results of all J' are superimposed to obtain a vibration peak.

It is assumed that the rotational and vibrational states of N_2 are both Maxwell–Boltzmann distributions, and each particle has a single rotational temperature and vibrational temperature. The line intensity of the N_2 can be expressed as

$$I_{B_{v''}J''}^{C_{v'}J'} = \frac{D}{\lambda^4} q_{v',v''} \exp(-E_{v'}/KT_v) H_{J',J''} \exp(-E_{J'}/KT_r) \quad (8)$$

The vibrational energy of the higher vibrational levels in the transition can be expressed as

$$E_{v'} = hc\omega_e \left(v' + \frac{1}{2} \right) - hc\omega_e x_e \left(v' + \frac{1}{2} \right)^2 \quad (9)$$

The rotational energy of the higher rotational energy level can be expressed as

$$E_{J'} = hcB_{v'} J' (J' + 1) \quad (10)$$

The broadening function of the spectral line is the same as that of the gas rotational temperature fitting. In the calculation, J' ranges from 0 to 40, considering the P, Q and R branches corresponding to each rotational quantum number. All rotational quantum numbers are added to the corresponding peaks to obtain the vibrational spectrum.

In this paper, the above fitting method is realized by an in-house code, and the wavelength spectrum of the N_2 ($C^3\Pi_u-B^3\Pi_g$) is selected and brought into the program to realize the diagnosis of the plasma rotational temperature.

Figure 6 shows the experimental data and fitting curve of the N_2 band under different equivalence ratios, and Table 4 shows the rotational temperature obtained by fitting the N_2 band. It can be seen from the figure that as the equivalence ratio increases gradually, the normalized value of the tail of the spectral band increases gradually, indicating that the rotational temperature rises. When the working gas is pure air, the rotational temperature obtained by fitting is about 1634 K, and the equivalence ratio is 0.2, the rotational temperature obtained by fitting is about 1716 K. When the equivalence ratio is 0.4, the rotational temperature obtained by fitting is about 1864 K. The increase in temperature helps to enhance the initial temperature of the mixed gas flow, which has a positive effect on the progress of NH_3 ignition and combustion reaction.

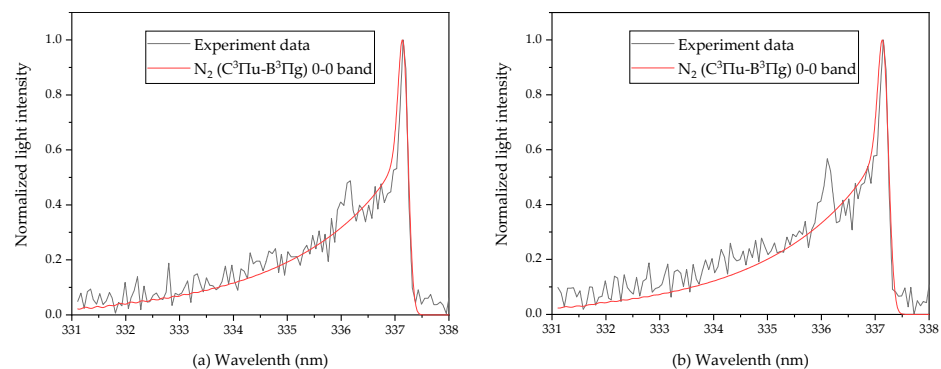


Figure 6. Fitting of N_2 ($C^3\Pi_u-B^3\Pi_g$) at equivalent ratio of (a) 0.3 and (b) 0.5.

Table 4. Rotational temperature obtained by fitting the N_2 ($C^3\Pi_u-B^3\Pi_g$) band.

EQR	0	0.1	0.2	0.3	0.4	0.5
T_R (± 100 K)	1634	1678	1716	1624	1864	1956

At the same time, in Figure 6, it can be seen that there is an obvious NH band near 336 nm, which overlaps with the tail of the N_2 band. It can be considered that the theoretical value of the N_2 band obtained by subtracting the total light intensity of the spectral band at the corresponding wavelength is the NH light intensity. It can be seen from the figure

that the ratio of NH to N₂ light intensity increases significantly with the increase of the equivalence ratio, indicating that the content of NH is gradually increasing.

Figure 7 shows the variation trend of NO content at the outlet position with the equivalence ratio recorded by the flue gas analyzer. As can be seen from the figure, it may be that the plasma contains more excited N and excited O species, thus more NO is generated through the plasma chemical reaction. At the same time, due to the high arc temperature of the gliding arc device, thermal NO will be generated [32], so a larger amount of NO will still be generated when discharging with pure air. However, with the addition of NH₃, the NO content showed a significant downward trend when the equivalence ratio did not reach the flammable range. The main reason was that NH₃ is excited to produce a series of excited species during the discharge process [33], and these species rapidly dissociate to produce excited NH₂ and H [34], at the same time, the generated NH₂ can further react to generate active radicals such as NH. NH₂ and NH can reduce the NO generated by the discharge and arc thermal effect through the reaction of R4, R5, etc. [35], thereby reducing the NO content at the outlet. When the equivalence ratio is 0.5, the NO content at the outlet increases sharply with the combustion of NH₃.

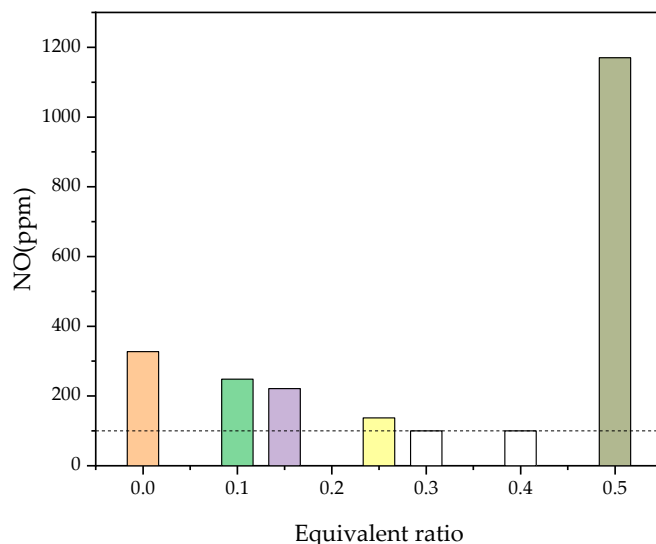


Figure 7. NO content at the outlet position under different equivalence ratios.

3.3. Spatial Distribution of Key Active Species

Figure 8 shows axial imaging pictures of swirl burner without filter. Figure 8a is the image of pure air discharge. It can be seen that the arc is generated at the bottom of the gliding arc device where the distance between the center electrode and the outer wall is small and develops upward to a larger space in the burner, forming a multi-layer arc structure close to the center. The light intensity near the electrode is significantly higher than that in the middle region, indicating that more fluorescent species are generated by discharge near the central electrode. Figure 8b is the image of the discharge plasma and the flame when the equivalence ratio is 0.5. It can be seen that the flame and the discharge plasma have a large difference in spatial structure. The gliding arc plasma is a multi-strand filament structure, while flame has a more uniform spatial distribution. It can be seen from Figure 8b that the image at the bottom of the burner still shows a filamentous structure, indicating that the NH₃ in this area has not yet started to burn, and it is mainly the plasma generated by the discharge. As the mixed gas flow continues to spin up, the image changes from the filamentary structure of the discharge to the continuous structure of the flame. At the same time, it can be seen that the flame also shows the characteristics of higher light intensity near the center electrode, the main reason may be that in this area,

more active species are generated due to the discharge, thus effectively strengthening the combustion reaction of NH_3 . Therefore, the intensity of combustion reaction in this region is significantly stronger than that in the middle and outer wall regions of the swirl burner.

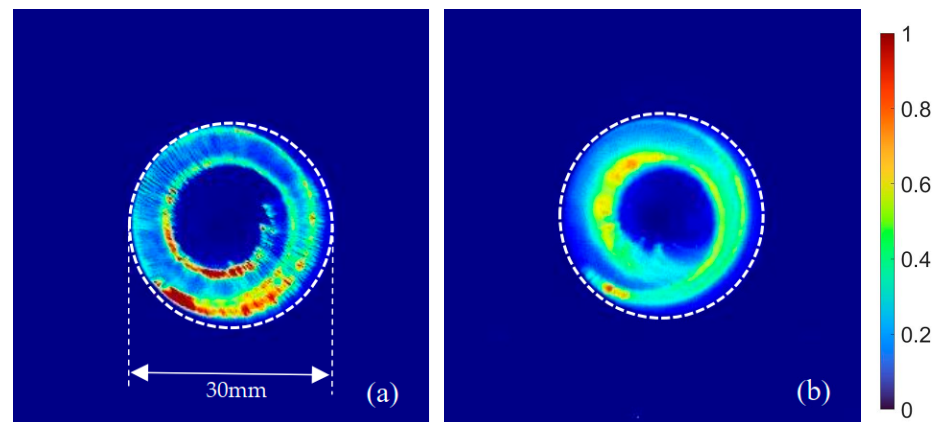


Figure 8. Axial imaging picture of swirl burner without filter, (a) pure air, (b) EQR = 0.5.

Figure 9 shows the axial imaging pictures of the swirl burner using different wavelength filters: a-c corresponds to a central wavelength of 660 nm and d-f corresponds to a central wavelength of 780 nm, corresponding to H_α and $\text{O}777$ spectral lines respectively. The color in the figure represents the normalized relative light intensity, 1 represents the strongest value of the light intensity, and 0 represents no light emission. It can be seen from the figure that when a small amount of ammonia is added to the gas mixture, the light intensity of H_α has been greatly improved in the overall space, and the light intensity of $\text{O}777$ has decreased slightly, but it is still obvious in the overall space. However, with the further increase of NH_3 , when the equivalence ratio is 0.5, the spatial distribution of them all decrease rapidly. The drop in $\text{O}777$ is the most significant, only a very small amount of distribution of $\text{O}777$ exist in the middle and lower parts of the burner, and the rest of the burner is basically unable to be observed. The spatial distribution of H_α is different from $\text{O}777$. It still maintains a large distribution in the middle and lower parts of the burner, but it shows a sharp downward trend as the mixed gas flow rises, and there is only a very weak filamentous shape in the upper part of the burner. The structure shows that the amount of H_α generated in the plasma is very small at this time, but there is still a small amount of H_α distribution near the inner wall, and the spatial distribution structure is irregular, this is mainly caused by the local expansion of the gas in the burner due to the heat released by the combustion reaction in the flame, so that affects the spatial characteristics of the discharge. In the experiment, we also found that when the equivalence ratio is 0.5, when the power supply of the gliding arc plasma generator is turned off, the ammonia swirling flame will be quickly extinguished. Therefore, the gliding arc plasma under this power can effectively broaden the lean burn limit.

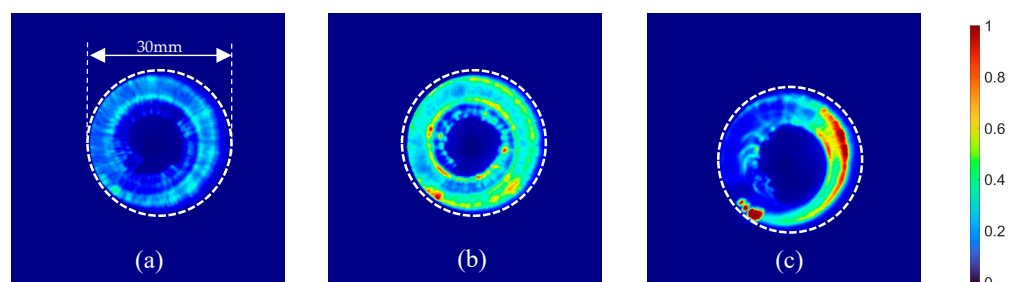


Figure 9. Cont.

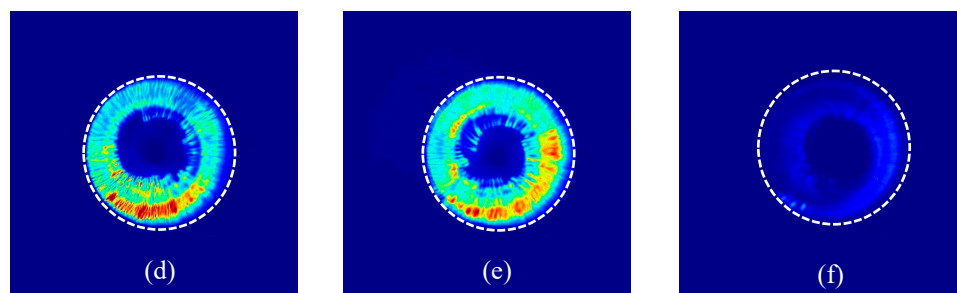


Figure 9. Axial imaging picture of swirl burner with filters, (a–c) 660 nm, (d–f) 780 nm, (a,d) pure air, (b,e) EQR = 0.1, (c,f) EQR = 0.5.

4. Conclusions

This work investigates the characteristics of ammonia premixed swirling flames assisted by gliding arc plasma.

Effective ignition can be achieved when the equivalence ratio is 0.5 with a low electrical power, which broadens the lean combustion limit of the ammonia swirl flame and has a better economy. At the same time, with the increase of NH_3 content, the width of the H_α line decreases significantly, indicating that the electron density shows a downward trend while the gas rotational temperature shows an upward trend. When the equivalence ratio was changed from 0.2 to 0.4, the gas temperature increased by about 200 K. The gliding arc plasma discharge can effectively promote the dissociation of NH_3 to generate H atoms, but as the equivalence ratio increases, the H atoms will be rapidly consumed, and with the increase of NH content, the reaction of ammonia will be further promoted, thereby enhancing the combustion of ammonia. The image results show that the content of O atoms generated by the discharge in the entire burner space will decrease rapidly with the increase of the equivalence ratio, while the content of H_α remains relatively high in the middle and lower parts of the burner and is rapidly consumed in its upper space. There is only an obvious distribution near the inner electrode, indicating that O777 has extremely high reactivity, and can quickly participate in the combustion reactions.

These results indicate that the gliding arc plasma can enhance the combustion performance of ammonia by generating a large number of O atoms and promoting ammonia dissociation.

Author Contributions: Conceptualization, X.Z. and Y.Z., methodology; X.Z. and B.H.; investigation, X.Z., Y.Z. and P.L., re-sources, X.Z., W.Z. and M.Z.; writing—original draft preparation, Y.Z. and X.Z., writing—review and editing, B.H. and X.Z., funding acquisition, B.H. and W.Z. All authors have read and agreed to the published version of the manuscript.

Funding: This work was supported by the National Natural Science Foundation of China (NSFC 91741204, NSFC 51907190).

Institutional Review Board Statement: Not applicable.

Informed Consent Statement: Not applicable.

Data Availability Statement: Not applicable.

Conflicts of Interest: The authors declare no conflict of interest.

References

1. Liu, Z.; Deng, Z.; Davis, S.J.; Giron, C.; Ciais, P. Monitoring global carbon emissions in 2021. *Nat. Rev. Earth Environ.* **2022**, *3*, 217–219. [[CrossRef](#)] [[PubMed](#)]
2. Yousefi, A.; Guo, H.; Dev, S.; Liko, B.; Lafrance, S. Effects of ammonia energy fraction and diesel injection timing on combustion and emissions of an ammonia/diesel dual-fuel engine. *Fuel* **2022**, *314*, 122723. [[CrossRef](#)]
3. Valera-Medina, A.; Xiao, H.; Owen-Jones, M.; David, W.; Bowen, P. Ammonia for power. *Prog. Energy Combust. Sci.* **2018**, *69*, 63–102. [[CrossRef](#)]
4. Morlanés, N.; Katikaneni, S.P.; Paglieri, S.N.; Harale, A.; Solami, B.; Sarathy, S.M.; Gascon, J. A technological roadmap to the ammonia energy economy: Current state and missing technologies. *Chem. Eng. J.* **2021**, *408*, 127310. [[CrossRef](#)]

5. Giddey, S.; Badwal, S.P.S.; Munnings, C.; Dolan, M. Ammonia as a renewable energy transportation media. *ACS Sustain. Chem. Eng.* **2017**, *5*, 10231–10239. [CrossRef]
6. Chang, F.; Gao, W.; Guo, J.; Chen, P. Emerging Materials and Methods toward Ammonia-Based Energy Storage and Conversion. *Adv. Mater.* **2021**, *33*, 2005721. [CrossRef] [PubMed]
7. Chai, W.S.; Bao, Y.; Jin, P.; Tang, G.; Zhou, L. A review on ammonia, ammonia-hydrogen and ammonia-methane fuels. *Renew. Sustain. Energy Rev.* **2021**, *147*, 111254. [CrossRef]
8. Berwal, P.; Kumar, S.; Khandelwal, B. A comprehensive review on synthesis, chemical kinetics, and practical application of ammonia as future fuel for combustion. *J. Energy Inst.* **2021**, *99*, 273–298. [CrossRef]
9. Lee, D.; Song, H.H. Development of combustion strategy for the internal combustion engine fueled by ammonia and its operating characteristics. *J. Mech. Sci. Technol.* **2018**, *32*, 1905–1925. [CrossRef]
10. Tang, Y.; Xie, D.; Shi, B.; Wang, N.; Li, S. Flammability enhancement of swirling ammonia/air combustion using AC powered gliding arc discharges. *Fuel* **2022**, *313*, 122674. [CrossRef]
11. Choe, J.; Sun, W.; Ombrello, T.; Carter, C. Plasma assisted ammonia combustion: Simultaneous NO_x reduction and flame enhancement. *Combust. Flame* **2021**, *228*, 430–432. [CrossRef]
12. Paulauskas, R.; Martuzevičius, D.; Patel, R.; Pelders, J.; Nijdam, S.; Dam, N.; Tichonovas, M.; Striūgas, N.; Zakarauskas, K. Biogas combustion with various oxidizers in a nanosecond DBD microplasma burner. *Exp. Therm. Fluid Sci.* **2020**, *118*, 110166. [CrossRef]
13. Mao, X.; Chen, Q.; Rousoo, A.C.; Chen, T.Y.; Ju, Y. Effects of controlled non-equilibrium excitation on H₂/O₂/He ignition using a hybrid repetitive nanosecond and DC discharge. *Combust. Flame* **2019**, *206*, 522–535. [CrossRef]
14. Zhang, Y.; Zhang, Y.-M.; Luo, K.; Yi, H.-L.; Wu, J. Electroconvective instability near an ion-selective surface: A mesoscopic lattice Boltzmann study. *Phys. Rev. E* **2022**, *105*, 055108. [CrossRef] [PubMed]
15. Luo, Y.; Gan, Y.; Jiang, Z. Study on the electrical response of small ethanol-air diffusion flame under the uniform electric field. *Int. J. Energy Res.* **2020**, *44*, 11872–11882. [CrossRef]
16. Wu, B.; Hastings, M.; Sun, W.; Ombrello, T.; Carter, C. Dynamics of laminar ethylene lifted flame with ozone addition. *Proc. Combust. Inst.* **2021**, *38*, 6773–6780. [CrossRef]
17. Gomez del Campo, F. Plasma-Assisted Control of Combustion Instabilities in Low-Emissions Combustors at Realistic Conditions. In Proceedings of the AIAA Propulsion and Energy 2019 Forum, Indianapolis, IN, USA, 19–22 August 2019; p. 3950.
18. Zhao, B.-B.; Chen, G.-C.; He, L.-M.; Jin, T.; Jing, B. Experimental investigation of plasma jet ignition characteristics in kerosene–air mixtures. *J. Aerosp. Eng.* **2020**, *33*, 04019113. [CrossRef]
19. Chen, W.; Jin, D.; Cui, W.; Huang, S. Characteristics of gliding arc plasma and its application in swirl flame static instability control. *Processes* **2020**, *8*, 684. [CrossRef]
20. Deng, K.; Zhao, S.; Xue, C.; Hu, J.; Zhong, Y.; Zhong, Y. Combustion Instability of Swirl Premixed Flame with Dielectric Barrier Discharge Plasma. *Processes* **2021**, *9*, 1405. [CrossRef]
21. Sorrentino, G.; Sabia, P.; de Joannon, M.; Bozza, P.; Ragucci, R. Influence of preheating and thermal power on cyclonic burner characteristics under mild combustion. *Fuel* **2018**, *233*, 207–214. [CrossRef]
22. Sarofim, A.F. *The John Zink Combustion Handbook*; Chemical Engineering. 2001, Volume 108, p. 10. Available online: <https://go.gale.com/ps/i.do?id=GALE%7CA76770443&sid=googleScholar&v=2.1&it=r&linkaccess=abs&issn=00092460&p=AONE&sw=w&userGroupName=anon%7E82a598f7> (accessed on 9 August 2022).
23. Song, J.; Wang, Z.; Cheng, X.; Wang, X. State-of-Art review of NO reduction technologies by CO, CH₄ and H₂. *Processes* **2021**, *9*, 563. [CrossRef]
24. Gordiets, B.; Ricard, A. Production of N, O and NO in N₂-O₂ flowing discharges. *Plasma Sources Sci. Technol.* **1993**, *2*, 158. [CrossRef]
25. Bonhommeau, D.; Valero, R.; Truhlar, D.G.; Jasper, A.W. Coupled-surface investigation of the photodissociation of NH₃ (\bar{A}): Effect of exciting the symmetric and antisymmetric stretching modes. *J. Chem. Phys.* **2009**, *130*, 234303. [CrossRef]
26. Zhu, X.-M.; Chen, W.-C.; Li, J.; Pu, Y.-K. Determining the electron temperature and the electron density by a simple collisional–radiative model of argon and xenon in low-pressure discharges. *J. Phys. D Appl. Phys.* **2008**, *42*, 025203. [CrossRef]
27. Zhu, X.M.; Pu, Y.K. Using OES to determine electron temperature and density in low-pressure nitrogen and argon plasmas. *Plasma Sources Sci. Technol.* **2008**, *17*, 024002. [CrossRef]
28. Zhu, X.-M.; Walsh, J.L.; Chen, W.-C.; Pu, Y.-K. Measurement of the temporal evolution of electron density in a nanosecond pulsed argon microplasma: Using both Stark broadening and an OES line-ratio method. *J. Phys. D Appl. Phys.* **2012**, *45*, 295201. [CrossRef]
29. Wang, Q.; Koleva, I.; Donnelly, V.M.; Economou, D.J. Spatially resolved diagnostics of an atmospheric pressure direct current helium microplasma. *J. Phys. D Appl. Phys.* **2005**, *38*, 1690. [CrossRef]
30. Balcon, N.; Aanesland, A.; Boswell, R. Pulsed RF discharges, glow and filamentary mode at atmospheric pressure in argon. *Plasma Sources Sci. Technol.* **2007**, *16*, 217. [CrossRef]
31. Phillips, D.M. Determination of gas temperature from unresolved bands in the spectrum from a nitrogen discharge. *J. Phys. D Appl. Phys.* **1976**, *9*, 507. [CrossRef]
32. Vervloessem, E.; Aghaei, M.; Jardali, F.; Hafezkhiani, N.; Bogaerts, A. Plasma-Based N₂ Fixation into NO_x: Insights from Modeling toward Optimum Yields and Energy Costs in a Gliding Arc Plasmatron. *ACS Sustain. Chem. Eng.* **2020**, *8*, 9711–9720. [CrossRef]

33. Yao, C.; Chen, S.; Wang, S.; Chang, Z.; Sun, A.; Mu, H.; Zhang, G.-J. Characteristics of atmospheric Ar/NH₃ DBD and its comparison with He/N₂ DBD. *J. Phys. D Appl. Phys.* **2018**, *51*, 225201. [[CrossRef](#)]
34. Yi, M.; Scheiner, S. Proton transfer between phenol and ammonia in ground and excited electronic states. *Chem. Phys. Lett.* **1996**, *262*, 567–572. [[CrossRef](#)]
35. Miller, J.A.; Smooke, M.D.; Green, R.M.; Kee, R.J. Kinetic modeling of the oxidation of ammonia in flames. *Combust. Sci. Technol.* **1983**, *34*, 149–176. [[CrossRef](#)]